Polyhedron 66 (2013) 171–178

Contents lists available at SciVerse ScienceDirect

Polyhedron

journal homepage: www.elsevier.com/locate/poly

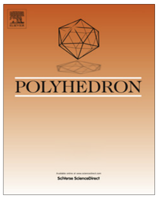

A Mn_4 single-molecule magnet with the defective-dicubane structure from the use of pyrenecarboxylic acid

Tu N. Nguyen, Khalil A. Abboud, George Christou *

Department of Chemistry, University of Florida, Gainesville, FL 32611-7200, United States

ARTICLE INFO

Article history:
Received 6 February 2013
Accepted 16 March 2013
Available online 30 March 2013

Keywords:
Manganese
Crystal structure
Single-molecule magnet
π–π Stacking

ABSTRACT

The reaction between $Mn(pc)_2{\cdot}4H_2O$ (pcH is 1-pyrenecarboxylic acid), N-methyldiethanolamine ($mdaH_2$), and NEt_3 in a 2:2:3 molar ratio in CH_2Cl_2 or $CHCl_3$ gives the tetranuclear complex $[Mn_4(pc)_4(mda)_2(mdaH)_2]$, isolated as the $\cdot 2CH_2Cl_2$ (**3**) and $\cdot 2CHCl_3$ (**4**) solvates, respectively. Only crystals of **4** were of sufficient quality for single-crystal X-ray crystallography. Complex **4** possesses a $[Mn^{II}_2Mn^{III}_2]$ core with the Mn ions arranged in a planar rhombus that can be described as two Mn_3 triangles fused at one edge. Additional monoatomic bridging by mda^{2-} or $mdaH^-$ μ- and μ_3-O atoms on each edge and at the center of the Mn_3 triangular units gives a defective-dicubane core structure. Ligation is completed by two bridging and two monodentate pc^- groups, each of which is involved in π–π stacking interactions with those on neighboring Mn_4 molecules to give a 2D network. Variable-temperature solid-state magnetic susceptibility studies of **3** and **4** in the temperature range 5.0–300 K. Various fitting and simulation models were employed in analyzing the data for **3**, which shows no evidence of significant intermolecular interactions, and it was concluded that it contains three symmetry-inequivalent exchange interactions, $J = +2.34\ cm^{-1}$, $J' = +7.70\ cm^{-1}$, $J'' = -1.33\ cm^{-1}$ and $g = 1.99$, where J' is the $Mn^{III}\cdots Mn^{III}$ interaction, and J and J'' are the $Mn^{II}\cdots Mn^{III}$ interactions. This indicates an $S = 8$ ground state with a very low-lying an $S = 9$ excited state. This conclusion was supported by fits of reduced magnetization data, which gave an $S = 8$ ground state with axial zero-field splitting parameter $D = -0.19(1)\ cm^{-1}$, and $g = 1.94(1)$. Ac susceptibility studies on **3** show that it is a single-molecule magnet (SMM). Complex **4** shows different magnetic behavior from **3** due to the intermolecular interactions.

1. Introduction

Single-molecule magnets (SMMs) are individual molecules that function as single-domain nanoscale magnetic particles below their blocking temperature, T_B [1]. This behavior arises from the combination of a large ground-state spin (S) and Ising-type magnetoanisotropy (negative zero-field splitting parameter, D), which leads to a significant energy barrier to the thermal relaxation of the molecular magnetic moment. The maximum energy barrier can be calculated by $S^2|D|$ or $(S^2-1/4)|D|$ for integer and half-integer spins, respectively. Experimentally, an SMM exhibits frequency-dependent out-of-phase ac magnetic susceptibility signals, and hysteresis in a plot of magnetization versus applied dc magnetic field [1]. Various families of SMMs have now been discovered, with the majority being homo- or heteronuclear Mn-complexes with the largest being a Mn_{84} torus [2]. SMMs have been shown to also display interesting quantum phenomena such as quantum tunneling of magnetization (QTM) [3] and quantum phase interference (QPI) [4]. Consequently, they have been proposed as qubits for quantum computation [5] and as components in molecular spintronics devices [6], which would exploit their quantum tunneling properties. For such applications, weak coupling of two or more SMMs to each other or to other components of a device are essential, while maintaining the intrinsic single-molecule properties of each SMM. The report of supramolecular C–H⋯Cl hydrogen-bonded pairs of $[Mn_4O_3Cl_4(O_2CEt)_3(py)_3]$ ($S = 9/2$) demonstrated such coupling between two SMMs for the first time, manifested as exchange-biased QTM steps, quantum superposition states, and quantum entanglement of the two SMMs [7,8]. Similarly, weak couplings were observed when four Mn_3 SMMs are connected by designed covalent linkers [9]. π–π Stacking is another type of weak bond that often (but not always [10]) provides weak magnetic interactions. There have been few studies of the effect of π–π stacking interactions on magnetic properties of SMMs. The recent report by Gao and coworkers demonstrated the first spin-canted supramolecular single-chain magnet by π–π stacking [11]. To extend our own work in this area, we have explored the synthesis of a known type of Mn_4 SMM containing large aromatic ligands to potentially introduce extensive π–π interactions between the molecules in the solid state. Among the known Mn_4 SMMs are $[Mn_4(O_2CPh)_4(mda)_2(mdaH)_2]$ (**1**)

---

* Corresponding author. Tel.: +1 352 392 8314; fax: +1 352 392 8757.
E-mail address: christou@chem.ufl.edu (G. Christou).

0277-5387/$ - see front matter © 2013 Elsevier Ltd. All rights reserved.
http://dx.doi.org/10.1016/j.poly.2013.03.041

($mdaH_2$ is N-methyldiethanolamine) and $[Mn_4(anca)_4(mda)_2(mdaH)_2]$ (**2**) (ancaH is anthracene-9-carboxylic acid), differing only in the size of the aromatic carboxylate [12]**.** Neither **1** nor **2** possess significant π–π stacking, and we therefore decided to explore the effect of significantly increasing the size of the carboxylate aromatic group. We chose pyrenecarboxylic acid (pcH) for this work because the pyrene group is well-known to give strong π–π stacking and has also been used for linking inorganic units to a graphene layer or carbon nanotube surface [13].

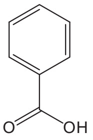

$PhCO_2H$

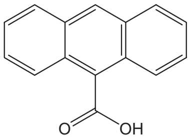

ancaH

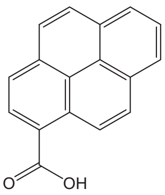

pcH

We herein describe the synthesis, structure and magnetic characterization of a Mn_4 SMM possessing pyrenecarboxylate ligation. We also describe the differing magnetic properties of the compound when prepared in CH_2Cl_2 or $CHCl_3$ solvent.

2. Experimental

2.1. Syntheses

All preparations were performed under aerobic conditions using materials and solvents as received. $Mn(pc)_2{\cdot}4H_2O$ was prepared from the reaction $MnCl_2$, sodium methoxide and pyrenecarboxylic acid in MeOH.

2.1.1. $[Mn_4(pc)_4(mda)_2(mdaH)_2]{\cdot}2CH_2Cl_2$ (3)

A solution of $Mn(pc)_2{\cdot}4H_2O$ (0.62 g, 1.0 mmol) in CH_2Cl_2 (30 ml) was treated with NEt_3 (0.21 ml, 1.5 mmol) and $mdaH_2$ (0.16 ml, 1.0 mmol). The solution was stirred for 1 h at room temperature, filtered and the brown filtrate left undisturbed. Crystals of **3** had formed after two days, and these were collected by filtration, washed with Et_2O and dried under vacuum. The yield was ~40%. The crystal quality was too poor for single-crystal X-ray crystallography. *Anal.* Calc. for **3** ($Mn_4O_{16}C_{90}H_{86}N_4Cl_4$): C, 58.71; H, 4.71; N, 3.04. Found: C, 58.92; H, 4.62; N, 2.95%. Selected IR data (cm^{-1}): 1596 (s), 1562 (s), 1534 (m), 1456 (w), 1389 (s), 1362 (m), 1322 (m), 1286 (s), 1151 (w), 1094 (m), 1066 (m), 1033 (w), 910 (w), 844 (m), 779 (w), 752 (w), 736 (w), 711 (w), 652 (w), 591 (w), 533 (w), 508 (w), 441 (w).

2.1.2. $[Mn_4(pc)_4(mda)_2(mdaH)_2]{\cdot}2CHCl_3$ (4)

A solution of $Mn(pc)_2{\cdot}4H_2O$ (0.62 g, 1.0 mmol) in $CHCl_3$ (30 ml) was treated with NEt_3 (0.21 ml, 1.5 mmol) and $mdaH_2$ (0.16 ml, 1.0 mmol). The solution was stirred for 1 hour at room temperature, filtered and the brown filtrate left undisturbed. X-ray quality crystals of **4** had formed after two days, and these were collected by filtration, washed with Et_2O and dried under vacuum. The yield was ~40%. *Anal.* Calc. for **4** ($Mn_4O_{16}C_{90}H_{84}N_4Cl_6$): C, 56.59; H, 4.43; N, 2.93. Found: C, 56.46; H, 4.33; N, 2.74%. Selected IR data (cm^{-1}): 1595 (s), 1562 (s), 1533 (m), 1456 (w), 1388 (s), 1360 (m), 1322 (m), 1286 (s), 1150 (w), 1094 (m), 1066 (m), 1030 (w), 911 (w), 842 (m), 779 (w), 751 (w), 734 (w), 711 (w), 652 (w), 591 (w), 533 (w), 508 (w), 441 (w).

2.2. General and physical measurements

Elemental analyses (C, H and N) were performed by the in-house facilities of the University of Florida Chemistry Department. Infrared spectra in the 400-4000 cm^{-1} range were recorded in the solid state (KBr pellets) on a Nicolet Nexus 670 FTIR spectrometer. Variable-temperature dc magnetic susceptibility data down to 5.0 K were collected using a Quantum Design MPMS-XL SQUID susceptometer equipped with a 7 Tesla dc magnet. Pascal's constants were used to estimate the diamagnetic corrections, which were subtracted from the experimental susceptibilities to give the molar magnetic susceptibilities (χ_M). Microcrystalline samples were restrained in eicosane by suspending the solid for 15 min in eicosane maintained at a temperature above its melting point (35–37 °C), and then the temperature was gradually decreased below the melting point to solidify the eicosane.

2.2.1. X-ray crystallography

Data were collected at 173 K on a Siemens SMART PLATFORM equipped with a CCD area detector and a graphite monochromator utilizing Mo Kα radiation (λ = 0.71073 Å). A suitable crystal of **4**·$2CHCl_3$ was attached to a glass fiber using silicone grease and transferred to a goniostat where it was cooled to 173 K for data collection. Cell parameters were refined 8192 reflections. A full sphere of data (1850 frames) was collected using the ω-scan method (0.3° frame-width). The first 50 frames were re-measured at the end of data collection to monitor instrument and crystal stability (maximum correction on I was <1%). Absorption corrections by integration were applied based on measured indexed crystal faces. The structure was solved by direct methods in SHELXTL6, and refined on F^2 using full-matrix least squares. The non-H atoms were treated anisotropically, whereas the H atoms were placed in calculated, ideal positions and were refined as riding on their respective C atoms. The asymmetric unit contains half the Mn_4 molecule and one $CHCl_3$ solvent of crystallization. A total of 543 parameters were included in the final refinement cycles using 6860 reflections with $I > 2\sigma(I)$ to yield R_1/wR_2 of 3.79/9.31%, respectively. Unit cell data and structure refinement details are listed in Table 1.

Table 1
Crystallographic data for complex **4**·$2CHCl_3$.

	4
Formula[a]	$C_{90}H_{84}Cl_6Mn_4N_4O_{16}$
Formula weight (g/mol)[a]	1910.16
Crystal system	triclinic
Space group	$P\bar{1}$
a (Å)	10.3338(3)
b (Å)	13.7303(4)
c (Å)	14.8169(5)
α (°)	84.332(2)
β (°)	82.443(2)
γ (°)	82.174(2)
V (Å^3)	2057.63(11)
Z	4
T (K)	100(2)
λ (Å)[b]	0.71073
ρ_{cal} (mg/m^3)	1.540
μ (mm^{-1})	0.867
R_1[c,d]	0.0379
wR_2[e]	0.0931

[a] Including solvent molecules.

[b] Graphite monochromator.

[c] $I > 2\sigma(I)$.

[d] $R_1 = \sum(||F_o| - |F_c||)/\sum|F_o|$.

[e] $wR_2 = [\sum[w(F_o^2 - F_c^2)^2]/\sum[w(F_o^2)^2]]^{1/2}$ where $w = 1/[\sigma^2(F_o^2) + (m{*}p)^2 + n{*}p]$, $p = [\max(F_o^2, 0) + 2{*}F_c^2]/3$, m and n are constants.

3. Results and discussion

3.1. Syntheses

Complexes **3** and **4** were prepared using procedures very slightly modified from those previously employed for **1** and **2** [12]. Owing to the higher solubility of $Mn(pc)_2{\cdot}4H_2O$ in CH_2Cl_2 and $CHCl_3$, the reactions were carried out directly in these solvents rather than MeCN as in the preparation of **1**. The procedure is summarized in Eq. (1-1), and involves oxidation of Mn^{II}

$$4Mn(O_2CR)_2 + 4mdaH_2 + 1/2O_2 \rightarrow [Mn_4(O_2CR)_4(mda)_2(mdaH)_2] + 4RCO_2H + H_2O \qquad (1\text{-}1)$$

by O_2 to give the mixed-valent $Mn^{II}{}_2Mn^{III}{}_2$ product. NEt_3 was also present to provide the basic conditions to facilitate aerial oxidation and to act as a proton acceptor; the same reactions but without NEt_3 lead to much slower darkening of the solution and a much lower yield of isolated **3** and **4**. X-ray quality, single crystals of **4**$\cdot 2CHCl_3$ were obtained from $CHCl_3$, but X-ray quality crystals from CH_2Cl_2 could not be obtained, even after numerous attempts when it was realized that **3** and **4** have distinctly different magnetic properties (*vide infra*) even though their Mn_4 molecules were concluded to be identical on the basis of the elemental analysis data and the near superimposability of their IR spectra.

3.2. Structural description of $[Mn_4(pc)_4(mda)_2(mdaH)_2]{\cdot}2CHCl_3$ (**4**)

A labeled structure of complex **4** and its core are shown in Fig. 1. Selected interatomic distances and angles are listed in Table 2. Complex **4** crystallizes in triclinic space group $P\bar{1}$ with the Mn_4 molecule lying on an inversion center. It contains a defective-dicubane $[Mn^{II}{}_2Mn^{III}{}_2\ (\mu_3\text{-}O)_2]$ core consisting of two edge-fused Mn_3 triangular units. The two mda^{2-} groups are each η^3-chelates to a Mn^{III} atom, Mn1, with one alkoxide O atom (O5) bridging to an adjacent Mn^{II} and the other alkoxide O (O6) triply-bridging a Mn_3 triangle. The two $mdaH^-$ groups are η^3-chelates to a Mn^{II} atom, with the alkoxide O atom (O7) bridging to a Mn^{III} and the protonated alcohol arm (O8) remaining terminal on the Mn^{II} (Mn2). Ligation is completed by two pc^- groups, each bridging a $Mn^{II}Mn^{III}$ pair, and a monodentate pc^- group on each Mn^{II}. The Mn^{III} ions are six-coordinate with distorted octahedral geometry, whereas the Mn^{II} ions are seven-coordinate. The Mn oxidation states and protonation levels of $mda^{2-}/mdaH^-$ O atoms were determined from bond valence sum (BVS) calculations (Tables 3 and 4), charge balance considerations, and the presence of Jahn-Teller (JT) distortions on the Mn^{III} ions (Fig. 1, bottom). There are two intramolecular hydrogen-bonds between the non-bound O atom (O4) of the terminal pc-groups and the protonated OH (O8) of the $mdaH^-$ chelates (O4···O8 = 2.644(3) Å). Inspection of the packing in **4** also reveals extensive π–π stacking of ~3.4 Å between pc^- groups on adjacent molecules: all four pc^- groups of each molecule of **4** are involved in these π–π interactions, which results in 2D layers of Mn_4 molecules (Fig. 2). These layers are not in registry, so there are no channels through the crystal (Fig. S1 of Supplementary material).

Further inspection of the packing rationalizes the elemental analysis data, which indicate that the two $CHCl_3$ solvent molecules are not lost on drying under vacuum. There are two evident reasons for this: (i) each $CHCl_3$ molecule is involved in a C–H···O hydrogen-bond with the $mdaH^-$ alcohol OH (O4) group (C45···O4 = 3.176(4) Å), which also rationalizes the absence of

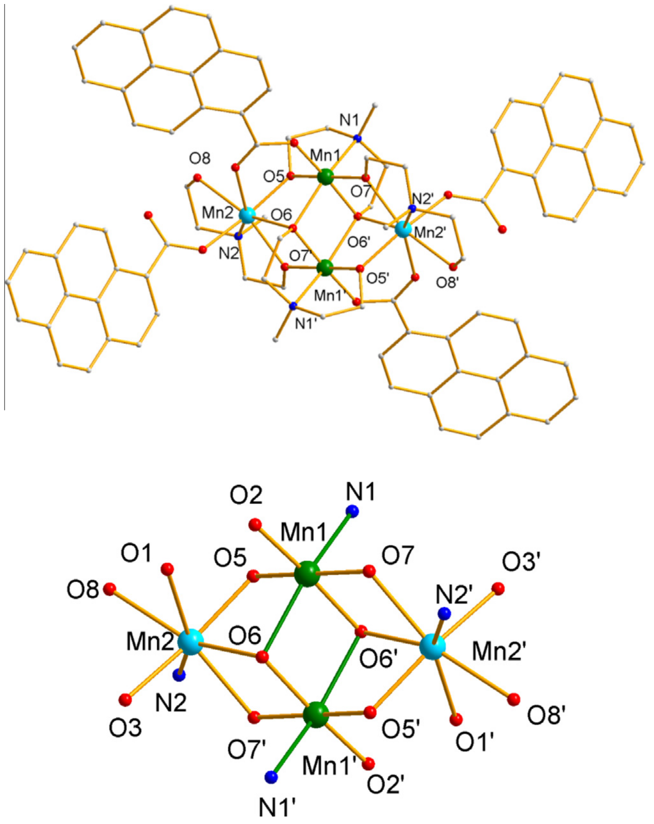

Fig. 1. The structure of complex **4** (top) and its core (bottom); H atoms and $CHCl_3$ solvent molecules have been omitted for clarity. The Mn^{III} JT elongation axes are shown as green bonds. Color code: Mn^{III} green, Mn^{II} sky blue, O red, N dark blue, C grey. (Color online).

Table 2
Selected bond distances (Å) and angles (°) for complex **4**.

Mn1–Mn1′	3.1676(6)	Mn2–O5	2.0825(15)
Mn1–Mn2	3.2058(5)	Mn2–O3	2.1080(15)
Mn1–O7	1.8740(16)	Mn2–O7′	2.2445(15)
Mn1–O5	1.9114(16)	Mn2–O8	2.3562(16)
Mn1–O2	1.9343(15)	Mn2–O6′	2.3673(16)
Mn1–O6	1.9570(15)	Mn2–N2	2.4130(20)
Mn1–O6′	2.2214(14)	Mn2–O1	2.4212(16)
Mn1–N1	2.3250(18)		
Mn1–O7–Mn2′	109.50(7)	Mn1–O6–Mn2	88.57(5)
Mn1–O6–Mn1′	99.01(6)	Mn1–O5–Mn2	106.69(7)
Mn1′–O6–Mn2	101.98(7)		

Table 3
Bond valence sums (BVS)[a] for the Mn atoms of **4**.

Atom	Mn(II)	Mn(III)	Mn(IV)
Mn1	3.21	**2.95**	3.08
Mn2	**1.88**	1.73	1.80

[a] The bold value is the one closest to the charge for which it was calculated; the oxidation state is the nearest integer to the bold value.

Table 4
Bond Valence Sums (BVS)[a] for selected O atoms of **4**.

Atom	BVS	Assignment
O5	1.97	O^{2-}
O6	1.95	O^{2-}
O7	1.92	O^{2-}
O8	1.09	OH^-

[a] The O atom is not protonated if the BVS is ~1.8–2.2, mono-protonated if ~1.0–1.4, and doubly-protonated if ~0.2–0.4.

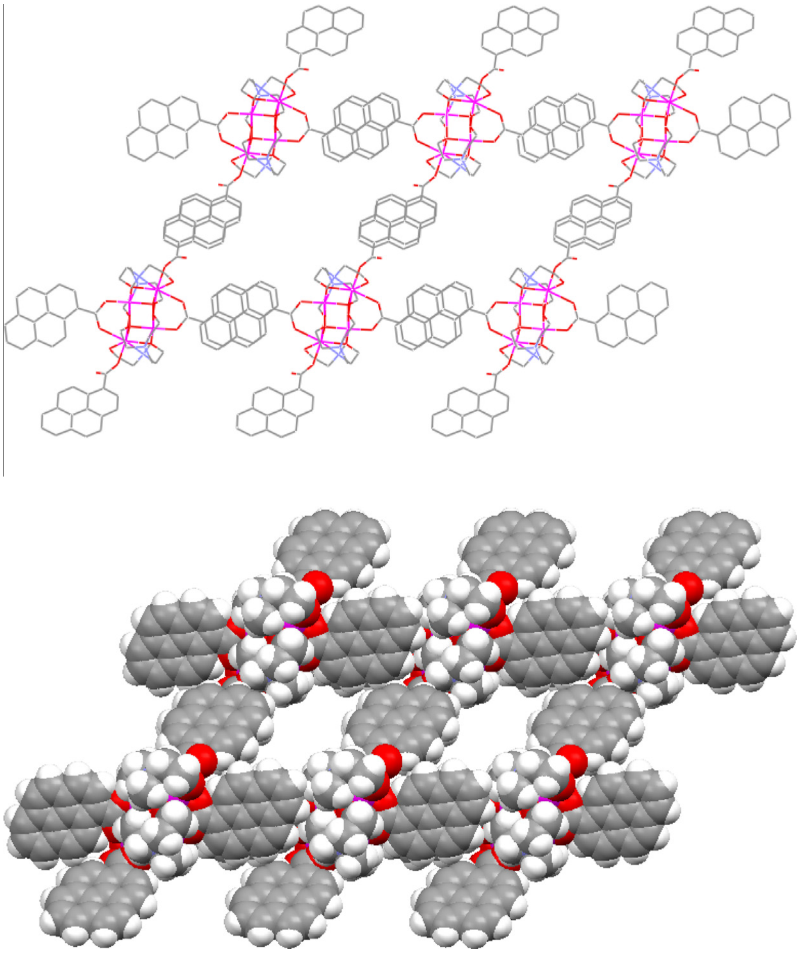

Fig. 2. The 2D network of complex **4** shown as stick (top) and spacefilling (bottom) representations.

any significant $CHCl_3$ disorder; and (ii) the $CHCl_3$ molecules are trapped within a cage-like space between three layers of Mn_4 molecules, completely enveloped by pc^- aromatic groups (Fig. S1). Two $CHCl_3$ solvent molecules were also reported to be retained in the structure of complex **2** after drying under vacuum [12b] even though it does not have a π–π stacked layer structure, as in **4**. The anthracene groups in **2** nevertheless are close to each other and can encapsulate the solvent molecules. Complex **3** is not believed to have the same π–π stacking layers as **4** (*vide infra*), but the elemental analysis data indicate retention of its two CH_2Cl_2 molecules after drying, probably analogous to **2**. As mentioned above, we could not obtain the crystal structure of **3** to probe this point further.

3.3. Magnetochemistry

3.3.1. DC Magnetic susceptibility studies

Variable-temperature, dc magnetic susceptibility (χ_M) measurements were performed on vacuum-dried polycrystalline samples of complexes **3** and **4** in an applied field of 1000 G (0.10 T) and in the 5.0–300 K temperature range. The samples were restrained in eicosane to prevent torquing. The obtained data are shown as $\chi_M T$ versus T plots in Fig. 3, and they are surprisingly different. For complex **3**, $\chi_M T$ increases from 15.57 $cm^3\,K\,mol^{-1}$ at 300 K to 32.08 $cm^3\,K\,mol^{-1}$ at 5.0 K. The 300 K value is close to the spin-only ($g = 2$) value for two Mn^{III} and two Mn^{II} non-interacting ions ($\chi_M T = 14.75\ cm^3\,K\,mol^{-1}$), and the $\chi_M T$ versus T profile indicates predominant ferromagnetic (F) interactions within the molecule. The 5 K value suggests that **3** may have an $S = 8$ ground state (spin-only value is 36 $cm^3\,K\,mol^{-1}$), similar to complex **2** [12b]. For complex **4**, $\chi_M T$ is 15.16 $cm^3\,K\,mol^{-1}$ at 300 K, slightly increasing to 16.16 $cm^3\,K\,mol^{-1}$ at 50 K and then decreasing to 10.25 $cm^3\,K\,mol^{-1}$ at 5.0 K. The plot for **3** is as expected for this kind of $Mn^{III}{}_2Mn^{II}{}_2$ cluster with the defective dicubane structure, so we rationalize the $\chi_M T$ versus T profile of **4** as due to the presence of intermolecular antiferromagnetic (AF) interactions propagated through the extensive π–π stacking in the crystal; each Mn_4 is interacting with four Mn_4 neighbors. A comparison of Mn–O–Mn bond angles within the Mn_4 core of **4** with those in **2**, which has an $S = 8$ ground state and a $\chi_M T$ versus T profile very similar to that of **3**, reveals that they are essentially identical (Fig. 4), supporting the presence of significant intermolecular interactions through the π–π stacking in **4**. As stated earlier, we were unsuccessful in multiple attempts to obtain the crystal structure of **3**, but its packing must be very different from **4**, with considerably fewer and weaker π–π contacts.

In order to obtain the exchange coupling parameters within the Mn_4 cluster, we fit the $\chi_M T$ versus T data of **3** to the appropriate theoretical expression. The core has virtual C_2 symmetry, so the four $Mn^{II}\cdots Mn^{III}$ interactions are not equivalent, and there are thus three different exchange couplings by symmetry – the central $Mn^{III}\cdots Mn^{III}$ and two different types of $Mn^{II}\cdots Mn^{III}$ couplings; the long distance $Mn^{II}\cdots Mn^{II}$ interaction is assumed to be zero. The HDVV spin Hamiltonian is given in Eq. (1-2), using the labeling of Figs. 1 and 3 (inset).

$$\mathcal{H} = -2J(\hat{S}_1\cdot\hat{S}_2 + \hat{S}_{1'}\cdot\hat{S}_{2'}) - 2J''(\hat{S}_1\cdot\hat{S}_{2'} - \hat{S}_{1'}\cdot\hat{S}_2) - 2J'(\hat{S}_1\cdot\hat{S}_{1'}) \tag{1-2}$$

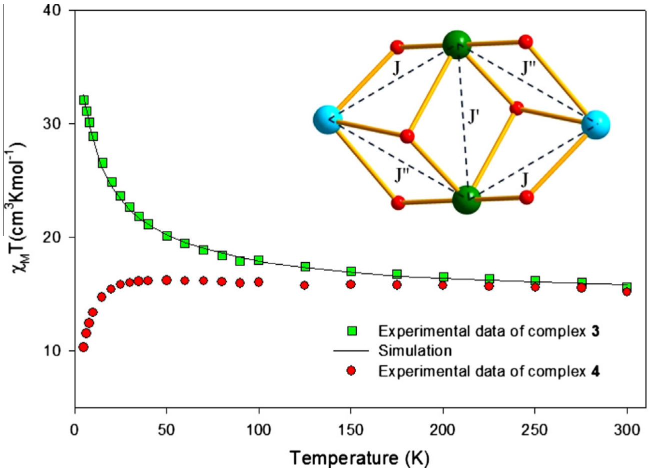

Fig. 3. Plot of $\chi_M T$ vs. T for complexes **3** and **4**. The solid line is the simulation to the 3-J coupling model shown as the inset. See the text for the parameters.

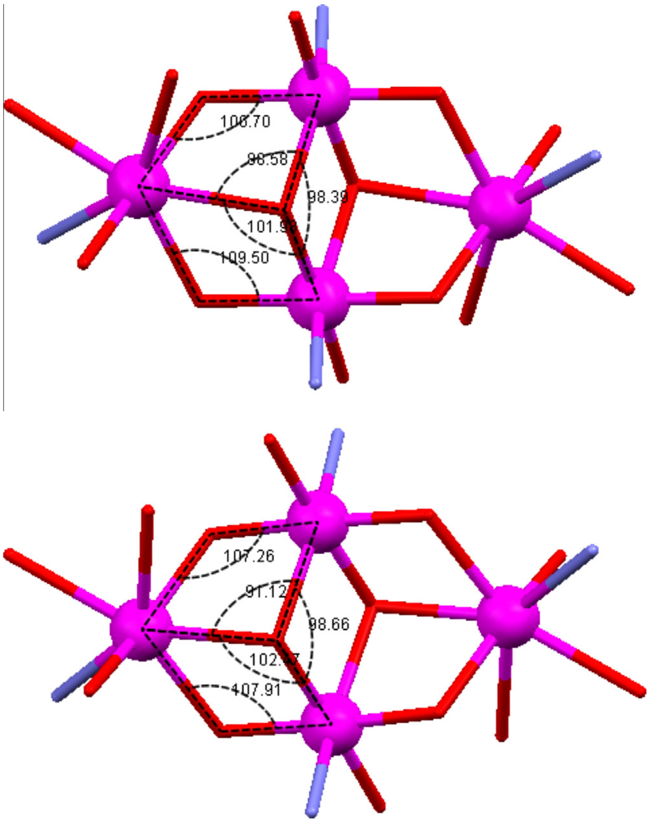

Fig. 4. Comparison of the core Mn–O–Mn angles in complexes **2** (bottom) and **4** (top).

However, as is typical for fits of data for defective-dicubanes, this 3-J system of C_2 symmetry is approximated as a 2-J system with C_{2v} core symmetry, i.e. the four $Mn^{II} \cdots Mn^{III}$ couplings are assumed to be equal ($J = J''$) [14]. The spin Hamiltonian is now given by Eq. (1-3), which can be converted into the equivalent form in Eq. (1-4) using the Kambe method, where

$$\mathcal{H} = -2J(\hat{S}_1 \cdot \hat{S}_2 + \hat{S}_{1'} \cdot \hat{S}_{2'} + \hat{S}_1 \cdot \hat{S}_{2'} + \hat{S}_{1'} \cdot \hat{S}_2) - 2J'(\hat{S}_1 \cdot \hat{S}_{1'}) \qquad (1\text{-}3)$$

$$\mathcal{H} = -J(\hat{S}_T^2 - \hat{S}_A^2 - \hat{S}_B^2) - J'(\hat{S}_A^2 - \hat{S}_1^2 - \hat{S}_{1'}^2) \qquad (1\text{-}4)$$

$\hat{S}_A = \hat{S}_1 + \hat{S}_{1'}, \hat{S}_B = \hat{S}_2 + \hat{S}_{2'}, and \hat{S}_T = \hat{S}_A + \hat{S}_B$; S_T is the total spin of the molecule, taking values of $S_T = 0–9$ since $S_1 = S_{1'} = 2$ and $S_2 = S_{2'} = {}^5/_2$. The eigenvalues of Eq. (1-4) are given by Eq. (1-5).

$$E(S_T, S_A, S_B) = -J[S_T(S_T+1) - S_A(S_A+1) - S_B(S_B+1)] \\ - J'[S_A(S_A+1)] \qquad (1\text{-}5)$$

A theoretical $\chi_M T$ versus T expression was derived using the Van Vleck equation and Eqs. (1-4) and (1-5), and including a fraction (p) of paramagnetic impurity and temperature-independent paramagnetism (TIP); the latter was kept constant at 600×10^{-6} cm^3 K mol^{-1}.

A good fit of this expression to the experimental data for **3** could only be achieved if certain constraints were applied: (i) omission of the two lowest-temperature data points (the best fit with all data gave $R^2 \sim 0.1$); (ii) restricting g to the 1.85–2.02 range (otherwise the best fit gave $R^2 \sim 0.7$ and $g \sim 3$; and (iii) keeping $J' < 0$ (the best fit for positive J' gave $R^2 \sim 0.5$). With all these constraints applied, a good fit ($R^2 = 0.999$) was obtained (Fig. S3 of Supplementary material) with $J = +2.53(7)$ cm^{-1}, $J' = -4.39\ (0.13)$ cm^{-1}, and $g = 2.00(1)$. However, a good fit is not always a realistic fit. The AF $J' = -4.39$ cm^{-1} is contrary to previous $[Mn^{II}_2Mn^{III}_2]$ molecules having this structure with μ_3-alkoxides, where the central Mn^{III} JT axes are in the central $\{Mn_2O_2\}$ plane and parallel, the d_z2 (d_σ) magnetic orbitals are orthogonal (Mn^{III}–O–Mn^{III} angles typically $\leqslant 100°$), and the coupling is therefore F. The structure of **3** is not available but related compound **4** has the expected orientation of JT axes and the Mn^{III}–O–Mn^{III} angle is 98.38(6)°, so J' is expected to be F. Thus, we rejected the obtained fit.

The assumption that the compound could be treated with a 2-J model (i.e. that $J = J''$ in sign and magnitude) was concluded to be unjustified, and that a 3-J treatment was necessary. The data were therefore treated with the C_2 symmetry 3-J model given by Fig. 3 (inset) and Eq. (1-2) using the program MAGPACK [15]. First, for comparison with the above analysis, we attempted to simulate the experimental data with the 2-J model but could not get a good MAGPACK simulation with $J' > 0$, in agreement with the Van Vleck fits. The best result is shown in Fig. S4 and gave $J = +0.34$ cm^{-1}, $J' = +12.00$ cm^{-1}, and $g = 1.97$.

The 2-J model ignores the fact that the two Mn^{II}–Mn^{III} coupling pathways are very different in the number of bridging ligands (3 versus 2) and their resulting Mn^{II}–O–Mn^{III} angles (average 97.64° versus 105.74°) (Fig 4, top), with the latter larger angles likely giving an AF interaction. Indeed, with the 3-J model a very good

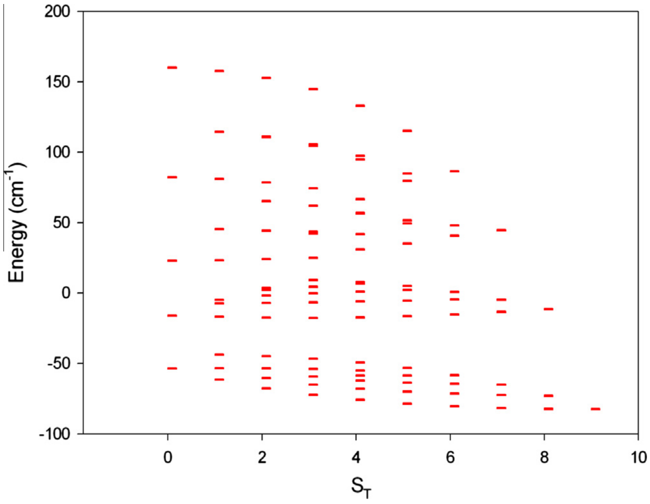

Fig. 5. Energy of the S_T states of **3** calculated with the parameters from the 3-J simulation. The ground state is $S_T = 8$, and a very low-lying $S_T = 9$ first excited state.

simulation was achieved with $J = +2.36\ \text{cm}^{-1}$, $J' = +7.70\ \text{cm}^{-1}$, $J'' = -1.32\ \text{cm}^{-1}$, and $g = 1.99$ (solid line in Fig. 3) with $R^2 = 0.96$. The simulation thus indicates both F and AF $\text{Mn}^{\text{II}}\cdots\text{Mn}^{\text{III}}$ couplings, consistent with the different structural parameters. Calculation of the S_T state energies (Fig. 5) gives an $S = 9$ ground state with $S = 8$ and $S = 7$ excited states at only 0.100 and $0.738\ \text{cm}^{-1}$, respectively, above the ground state. The tiny $S = 9$ versus $S = 8$ difference is within the parameter uncertainties: for example, a comparable quality simulation ($R^2 = 0.96$) was obtained with $J = +2.34\ \text{cm}^{-1}$, $J' = +7.70\ \text{cm}^{-1}$, $J'' = -1.33\ \text{cm}^{-1}$ and $g = 1.99$ (Fig. S5). In this case, however, the ground state is $S = 8$ with $S = 9$ and $S = 7$ excited states at 0.002 and $0.536\ \text{cm}^{-1}$, respectively. We thus conclude that the two lowest $S = 8$ with $S = 9$ states are very close in energy and it is not possible just on the basis of the MAGPACK results to determine the true ground state.

In order to probe the above point further, we collected magnetization (M) data for **3** in the 0.1–7 T and 1.8–10 K ranges, and these are plotted as $M/N\mu_B$ versus H/T in Fig. 6, where N is Avogadro's number, H is the applied field, and μ_B is the Bohr magneton. The data were fit using the program MAGNET [16] by diagonalization of the spin Hamiltonian matrix, incorporating axial anisotropy ($D\hat{S}_z^2$) and Zeeman terms, and employing a full powder average. The spin Hamiltonian is given by Eq. (1-6), where D is the axial ZFS parameter, and μ_0 is the vacuum permeability.

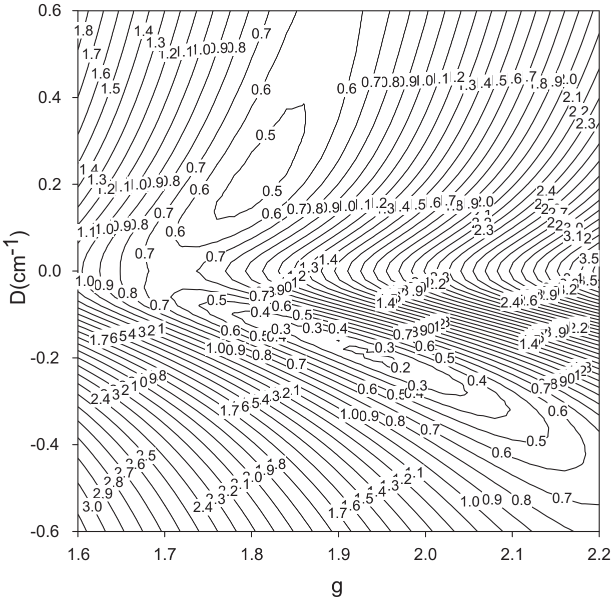

Fig. 7. Root-mean-square D vs. g error surface for the fit in Fig. 6 (top) shown as a 2D contour plot.

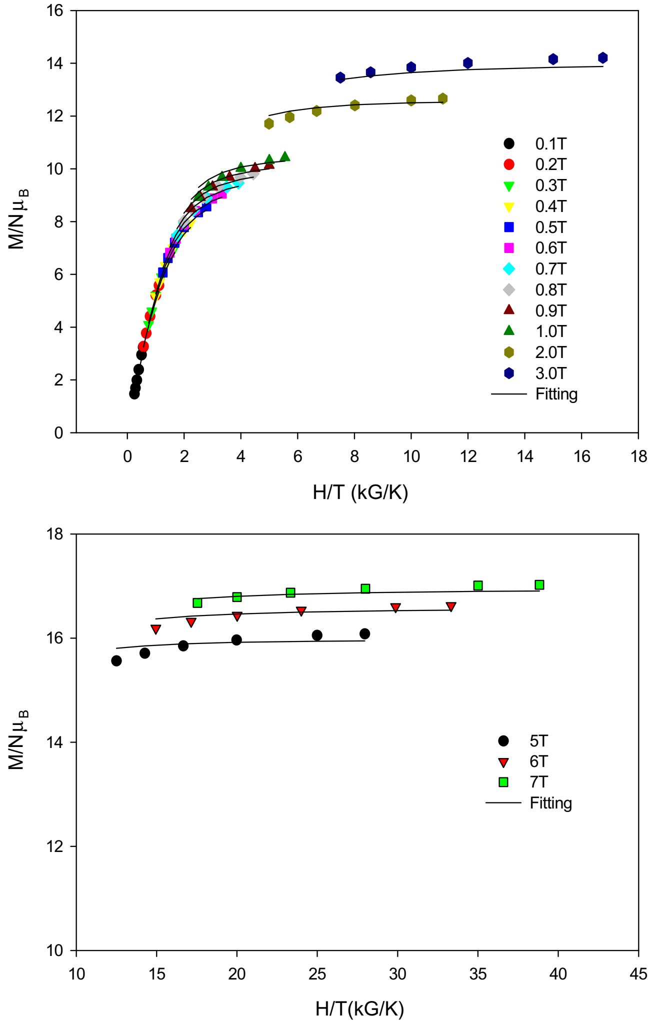

Fig. 6. Fits of reduced magnetization (M/μ_B) vs. H/T data for complex **3** collected in the (top) 1.8–4 K and 0.1-3.0 T ranges, and (bottom) 1.8–4 K and 5.0–7.0 T ranges. The solid lines are the fit of the data; see the text for the fit parameters.

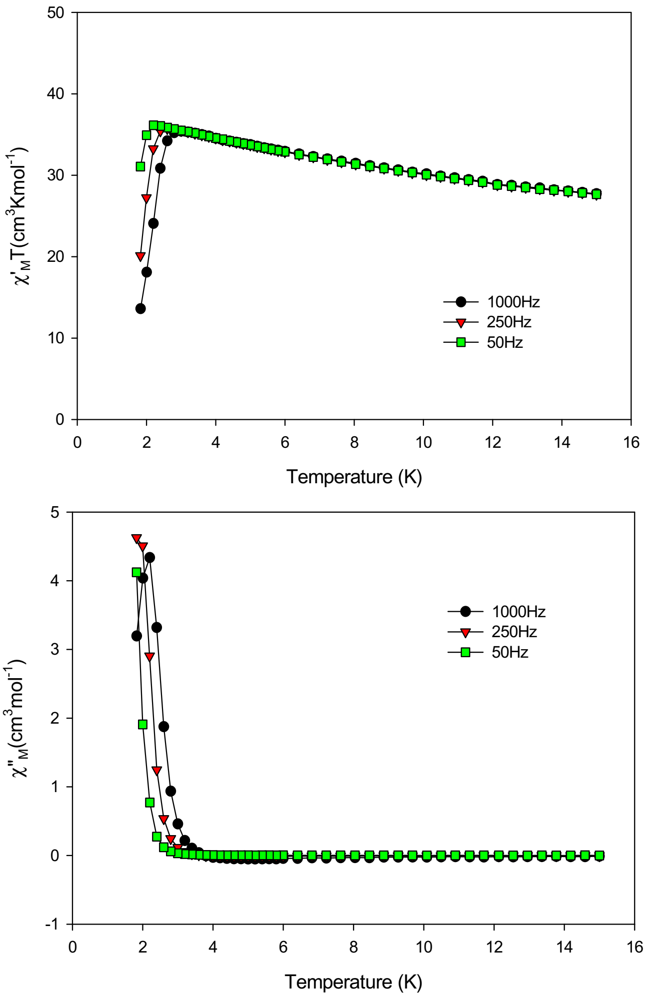

Fig. 8. Plot of the in-phase ($\chi'_M T$) and out-of-phase (χ'') ac susceptibility signals vs. temperature for **3** at the indicated frequencies.

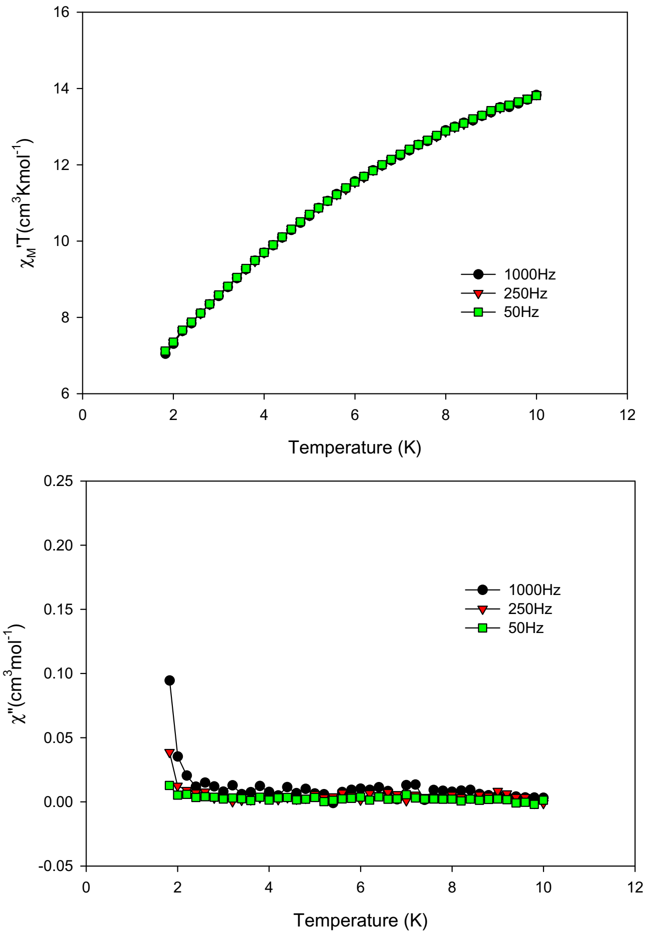

Fig. 9. Plot of the in-phase (χ'_MT) and out-of-phase (χ'') ac susceptibility signals vs temperature for **4** at the indicated frequencies.

$$\mathcal{H} = D\hat{S}_z^2 + g\mu_B\mu_0\hat{S}\cdot H \qquad (1\text{-}6)$$

No acceptable fit was obtained using the entire data set, as expected for very low-lying excited states because the program assumes only the ground state is populated. Using only data at the lower fields (0.1 T–3 T) and temperatures (1.8–4.0 K) to minimize population of the first excited state (Fig. 6, top) gave a reasonable fit with $S = 8$, $D = -0.19(1)\ \text{cm}^{-1}$, and $g = 1.94(1)$. Alternative fits for $S = 7$ or $S = 9$ gave $g = 2.20(1)$ and 1.73(1), respectively, which are unreasonable for Mn$^{\text{II/III}}$ complexes. The root-mean-square D versus g error surface for the fit (Fig. 7), calculated using the program GRID [16], showed another fit minimum with $S = 8$, $g = 1.81(1)$ and $D = +0.20(1)\ \text{cm}^{-1}$, but this fit with positive D and very low g was of much poorer quality. If $S = 8$ and $S = 9$ are the ground and excited states, respectively, then magnetization data at large fields should fit to an $S = 9$ state as this is stabilized below $S = 8$ by the large applied field. In agreement with this prediction, a good fit of only the data collected at 5–7 T and 1.8–4.0 K was obtained with $S = 9$, $D = -0.30(2)\ \text{cm}^{-1}$, and $g = 1.98(2)$ (Fig. 6, bottom). We thus conclude that **3** has an $S = 8$ ground state with $D = -0.19(1)\ \text{cm}^{-1}$, $g = 1.94(1)$, and a very low-lying $S = 9$ first excited state.

3.4. AC Magnetic susceptibility studies

Alternating current (ac) magnetic susceptibility measurements were performed on **3** and **4** in the 1.8–15 K range in a 3.5 G ac field oscillating at 50–1000 Hz, and the in-phase (χ'_M, as χ'_MT versus T) and out-of-phase (χ''_M versus T) data are shown in Figs. 8 and 9, respectively. The in-phase χ'_MT versus T for **3** increases with decreasing temperature, consistent with depopulation of excited states with smaller S_T values, and extrapolates to ~38 cm^3 K mol^{-1} at 0 K if the frequency-dependent decrease below ~3 K is ignored. The values for $S = 9$ and $S = 8$ with $g = 2.0$ are 45 and 36 cm^3 K mol^{-1}, and slightly less for $g < 2$ as expected for Mn$^{\text{III}}$-containing species. The extrapolated value at 0 K, if assumed to come from population of only one state, would be consistent with an $S = 9$ ground state with a very low $g = 1.84$, but this is disfavored because of the low g and the fact that it contradicts the other data. The extrapolated value is, however, in agreement with the value for an $S = 8/S = 9$ pair with very similar energies: for comparison, a degenerate $S = 8/S = 9$ pair with $g = 1.94$ would give $\chi'_MT = 38.3$ cm^3 K mol^{-1}. Thus, the ac data are consistent with the conclusion from the analysis of dc data that **3** has an $S = 8$ ground state with a very low-lying $S = 9$ excited state. The rapid frequency-dependent decrease in χ'_MT at <3 K and the corresponding appearance of out-of-phase χ''_M signals are indicative of slow magnetization relaxation, i.e. that **3** is a SMM. This is a typical behavior for this structural type of complex, where the large ground state spin and significant molecular anisotropy resulting from the two parallel Mn$^{\text{III}}$ JT axes together lead to significant barrier (vs kT) to magnetization relaxation.

For complex **4**, the in-phase ac data cannot be used to obtain the ground state because the χ'_MT is significantly decreased due to the intermolecular interactions, and is still rapidly decreasing below 10 K. There is still a very weak out-of-phase χ''_M signal.

4. Conclusions

Pyrenecarboxylic acid (pcH) has been successfully used in the synthesis of a new member of the Mn$^{\text{II}}_2$Mn$^{\text{III}}_2$ family of complexes with a defective-dicubane core. The compound has been crystallized from CH_2Cl_2 or $CHCl_3$, and distinctly different magnetic properties have been observed for the two solvate forms **3** and **4**, respectively. The former has the magnetic data characteristic of previous Mn$_4$ complexes of this type with $S = 8$ or $S = 9$ ground states, and displays the slow magnetization relaxation of an SMM. The latter displays extensive π–π stacking to give a network structure, and its magnetic properties are consistent with intermolecular AF interactions between Mn$_4$ units. The difference in packing between the two solvates emphasizes again how even small solvent differences can lead to significantly different solid-state properties, which in turn can have significant effects on the observed magnetic properties of SMMs. Further studies are in progress.

Acknowledgements

This work was supported by the National Science Foundation (DMR-1213030). T.N.N. thanks the Vietnam Education Foundation for a fellowship.

Appendix A. Supplementary data

CCDC 923210 contains the supplementary crystallographic data for **4**·2CHCl$_3$. These data can be obtained free of charge via http://www.ccdc.cam.ac.uk/conts/retrieving.html, or from the Cambridge Crystallographic Data Centre, 12 Union Road, Cambridge CB2 1EZ, UK; fax: +44 1223 336 033; or e-mail: deposit@ccdc.cam.ac.uk. Supplementary data associated with this article can be found, in the online version, at http://dx.doi.org/10.1016/j.poly.2013.03.041.

References

[1] (a) R. Sessoli, D. Gatteschi, A. Caneschi, M.A. Novak, Nature 365 (1993) 141;
(b) R. Sessoli, H.L. Tsai, A.R. Schake, S. Wang, J.B. Vincent, K. Folting, D. Gatteschi, G. Christou, D.N. Hendrickson, J. Am. Chem. Soc. 115 (1993) 1804;
(c) G. Christou, D. Gatteschi, D.N. Hendrickson, R. Sessoli, MRS Bull. 25 (2000) 66;
(d) G. Christou, Polyhedron 24 (2005) 2065;
(e) G. Aromi, E.K. Brechin, Struct. Bonding (Berlin) 122 (2006) 1;
(f) R. Bagai, G. Christou, Chem. Soc. Rev. 38 (2009) 1011.

[2] A.J. Tasiopoulos, A. Vinslava, W. Wernsdorfer, K.A. Abboud, G. Christou, Angew. Chem., Int. Ed. 10 (2004) 5180.

[3] (a) J.R. Friedman, M.P. Sarachik, J. Tejada, R. Ziolo, Phys. Rev. Lett. 76 (1996) 3830;
(b) L. Thomas, L. Lionti, R. Ballou, D. Gatteschi, R. Sessoli, B. Barbara, Nature 383 (1996) 145.

[4] (a) W. Wernsdorfer, R. Sessoli, Science 284 (1999) 133;
(b) W. Wernsdorfer, M. Soler, G. Christou, D.N. Hendrickson, J. Appl. Phys. 91 (2002) 7164;
(c) W. Wernsdorfer, N.E. Chakov, G. Christou, Phys. Rev. Lett. 95 (2005) 037203.

[5] (a) M.N. Leuenberger, D. Loss, Nature 410 (2001) 789;
(b) B. Zhou, R. Tao, S.-Q. Shen, J.-Q. Liang, Phys. Rev. A 66 (2002) 010301;
(c) M. Affronte, F. Troiani, A. Ghirri, A. Candini, M. Evangelisti, V. Corradini, S. Carretta, P. Santini, G. Amoretti, F. Tuna, G. Timco, R.E.P. Winpenny, J. Phys. D: Appl. Phys. 40 (2007) 2999;
(d) R. Vincent, S. Klyatskaya, M. Ruben, W. Wernsdorfer, F. Balestro, Nature 488 (2012) 357.

[6] (a) L. Bogani, W. Wernsdorfer, Nat. Mater. 7 (2008) 179;
(b) K. Katoh, H. Isshiki, T. Komeda, M. Yamashita, Chem. Asian J. 7 (2012) 1154.

[7] W. Wernsdorfer, N. Aliaga-Alcalde, D.N. Hendrickson, G. Christou, Nature 416 (2002) 406.

[8] (a) S. Hill, R.S. Edwards, N. Aliaga-Alcalde, G. Christou, Science 302 (2003) 1015;
(b) R. Tiron, W. Wernsdorfer, D. Foguet-Albiol, N. Aliaga-Alcalde, G. Christou, Phys. Rev. Lett. 91 (2003) 227203.

[9] T.N. Nguyen, W. Wernsdorfer, K.A. Abboud, G. Christou, J. Am. Chem. Soc. 133 (2011) 20688.

[10] T. Cauchy, E. Ruiz, O. Jeannin, M. Nomura, M. Fourmigue, Chem. Eur. J. 13 (2007) 8858.

[11] M. Ding, B. Wang, Z. Wang, J. Zhang, O. Fuhr, D. Fenske, S. Gao, Chem. Eur. J. 18 (2012) 915.

[12] (a) D. Foguet-Albiol, T.A. O'Brien, W. Wernsdorfer, B. Moulton, M.J. Zaworotko, K.A. Abboud, G. Christou, Angew. Chem., Int. Ed. 44 (2005) 897;
(b) C.C. Beedle, C.J. Stephenson, K.J. Heroux, W. Wernsdorfer, D.N. Hendrickson, Inorg. Chem. 47 (2008) 10798.

[13] (a) L. Bogani, C. Danieli, E. Biavardi, N. Bendiab, A.-L. Barra, E. Dalcanale, W. Wernsdorfer, A. Cornia, Angew. Chem., Int. Ed. 48 (2009) 746;
(b) S. Kyatskaya, J.R.G. Mascaros, L. Bogani, F. Hennrich, M. Kappes, W. Wernsdorfer, M. Ruben, J. Am. Chem. Soc. 131 (2009) 15143;
(c) C. Danieli, A. Cornia, C. Cecchelli, R. Sessoli, A.-L. Barra, G. Ponterini, B. Zanfrognini, Polyhedron 28 (2009) 2029;
(d) M. Lopes, A. Candini, M. Urdampilleta, A. Reserbat-Plantey, V. Bellini, S. Klyatskaya, L. Marty, M. Ruben, M. Affronte, W. Wernsdorfer, N. Bendiab, ACS Nano 4 (2010) 7531;
(e) Z. Xu, N.J. Singh, J. Lim, J. Pan, H.N. Kim, S. Park, K.S. Kim, J. Yoon, J. Am. Chem. Soc. 131 (2009) 15528;
(f) D.-W. Lee, T. Kim, M. Lee, Chem. Commun. 47 (2011) 8259;
(g) P.D. Tran, A.L. Goff, J. Heidkamp, B. Jousselme, N. Guillet, S. Palacin, H. Dau, M. Fontecave, V. Artero, Angew. Chem., Int. Ed. 50 (2011) 1371;
(h) S. Ghosh, X. An, R. Shah, D. Rawat, B. Dave, S. Kar, S. Talapatra, J. Phys. Chem. C 116 (2012) 20688.

[14] (a) J. Yoo, E.K. Brechin, A. Yamaguchi, M. Nakano, J.C. Huffman, A.L. Maniero, L.-C. Brunel, K. Awaga, H. Ishimoto, G. Christou, D.N. Hendrickson, Inorg. Chem. 39 (2000) 3615;
(b) E.C. Sanudo, V.A. Grillo, J. Yoo, J.C. Huffman, J.C. Bollinger, D.N. Hendrickson, G. Christou, Polyhedron 20 (2001) 1269;
(c) E.C. Sanudo, V.A. Grillo, M.J. Knapp, J.C. Bollinger, J.C. Huffman, D.N. Hendrickson, G. Christou, Inorg. Chem. 41 (2002) 2441;
(d) A.M. Ako, V. Mereacre, I.J. Hewitt, R. Clerac, L. Lecren, C.E. Anson, A.K. Powell, J. Mater. Chem. 16 (2006) 2579;
(e) O. Roubeau, R. Clerac, Eur. J. Inorg. Chem. (2008) 4325.

[15] J.J. Borras-Almenar, J.M. Clemente-Juan, E. Coronado, B.S. Tsukerblat, J. Comput. Chem. 22 (2001) 985.

[16] E.R. Davidson, MAGNET, Indiana University, Bloomington, IN, 1999.